Article

JOURNAL OF
REINFORCED
PLASTICS &
COMPOSITES

Journal of Reinforced Plastics and Composites
30(19) 1655–1669

DOI: 10.1177/0731684411418549
jrp.sagepub.com

SAGE

Interlaminar fracture analysis in the $G_I - G_{II} - G_{III}$ space using prestressed transparent composite beams

András Szekrényes

Abstract

This work presents the mixed mode I/II/III prestressed split-cantilever beam specimen for the fracture testing of composite materials. The newly designed system is the superposition of the mode-I double-cantilever beam, mode-II end-loaded split, and mode-III modified split-cantilever beam specimens. The three fracture modes are combined by prestressing the mode-I and mode-II energy release rates at the same time, while the mode-III loading is provided by a testing machine. It is shown that the system is able to provide any combinations of the mode-I, mode-II, and mode-III energy release rates. The applicability and the limitations of the novel fracture mechanical test are demonstrated using unidirectional glass/polyester composite specimens. The experimental data is reduced by the virtual crack-closure technique. It is shown that the energy release rates are non-uniformly distributed along the crack front which involves that the model results must be evaluated pointwise, and initiation was expected at the point where the highest total energy release rate appeared. Finally, based on the present and previous results, a three-dimensional fracture surface was determined in the $G_I - G_{II} - G_{III}$ space.

Keywords

mixed-mode delamination, double-cantilever beam, end-loaded split, modified split-cantilever beam

Introduction

The delamination fracture analysis of fiber-reinforced composite materials has a considerably huge literature, of which major part deals with mode-I, mode-II, and combined I/II cases.[1,2] Linear elastic fracture mechanics (LEFM) (e.g. Ref. 3) implies even the third (or tearing) fracture mode, which has significance in edge delamination[4] and delamination buckling effects.[5] In the last years, many articles were published on mode-III, first of all the development of new test methods should be emphasized. Compared to the standard mode-I and mode-II tests, mode-III involves significant difficulties, such as the complex fixtures, difficult specimen preparation, and data reduction. Based on the state-of-art review of the literature, the following fracture tests are available for mode-III testing of fiber-reinforced composites:

- the crack rail shear (CRS) test,[6]
- the split-cantilever beam (SCB),[7–9]
- the edge-crack torsion (ECT) test,[10–17]
- the modified version of the split-cantilever beam,[18–22]
- the anticlastic plate bending (APCB) method,[23,24]
- the mode-III four point-bend end-notched flexure ($4ENF_{III}$),[25]
- the four-point bending plate (4PBP) test,[26]
- the updated version of the modified split-cantilever beam,[27]
- the six-point edge crack torsion (6ECT),[28] and
- the shear-torsion-bending (STB) test.[29]

Department of Applied Mechanics, Budapest University of Technology and Economics, Budapest, Hungary.

Corresponding author:
András Szekrényes, Department of Applied Mechanics, Budapest University of Technology and Economics, H-1111 Budapest, Müegyetem rkp. 5, Building MM, Hungary
Email: szeki@mm.bme.hu

Neither one seems to be perfect, although they work more or less correctly. When a mode-III system is to be chosen, one of the aspects can be whether the system is extendable for mixed-mode I/III, II/III, and I/II/III conditions or not. From this point of view, the composite literature offers the following configurations:

- prestressed end-notched flexure ($PENF_{II/III}$),[30]
- the eight-point bending plate (8PBP, mixed-mode I/III) system,[31]
- the six-point bending plate (6PBP, mixed-mode II/III) system,[32]
- the prestressed split-cantilever beam ($PSCB_{I/III}$),[33]
- the double-notched split cantilever beam (DNSCB, mixed-mode II/III),[34]
- prestressed split-cantilever beam ($PSCB_{II/III}$),[35]
- the shear-torsion-bending test (STB).[29]

The $PENF_{II/III}$ specimen[30] is based on the superposition of the mode-II end-notched flexure (ENF) and the mode-III modified split-cantilever beam (MSCB) systems.[27] Its 'twin brothers' are the $PSCB_{I/III}$[33] and $PSCB_{II/III}$[35] systems, double-cantilever beam (DCB) + MSCB and end-loaded split (ELS) + MSCB combinations, respectively, which all together apply the traditional beam-like specimen geometry. The distribution of the energy release rates (ERR) is non-uniform along the crack front of the specimens due to the combined bending-shearing-torsion loading. Self-similarity is not achieved, therefore the ERR must be evaluated pointwise in these systems. As an advantage, the complete $G_I - G_{III}$, $G_{II} - G_{III}$ planes can be covered by this system. The 8PBP[31] and 6PBP[32] systems involve the bending of delaminated composite plates, which requires much effort from the point of view of the test preparation. It has been shown that there is an almost constant mode ratio area, where self-similar crack propagation is expected. The measured data is reduced by the cohesive zone model and the virtual crack-closure technique. The DNSCB test[34] eliminates the torsional deformation applying a double-notched beam-like specimen. This system is suitable to perform crack propagation tests; however, the complete range of the ratios of G_{II} and G_{III} cannot be covered. The newest development is the STB test,[29] which involves a loading fixture similar to the mixed-mode bending (MMB)[36] and the MSCB systems. The method seems to be promising for the measurement of the mode-III toughness; however, its extension for mixed-mode I/III, II/III, and I/II/III cases is still in the early stages.[29] Moreover, the method applies edge-cracked specimens, the load-displacement response is slightly non-linear, and the crack length is restricted by the central load introductor.

In this work, the extended version of the PSCB, namely the $PSCB_{I/II/III}$ system, is developed, which makes it possible to test the composite material under I/II/III loading conditions. The new setup is based on the combination of the DCB, ELS, and MSCB systems. The basic concept is shown in Figure 1. The mode-I ERR is provided by a steel roller with constant diameter, while the mode-II loading is induced by an ELS setup with constant displacement imposition. Finally, the mode-III ERR is increased up to fracture initiation by a testing machine. It will be shown that specimens with relatively large crack lengths can be tested. The applicability and the advantages/drawbacks of the test are demonstrated by finite element calculations and experiments. Based on the reduced experimental data, the fracture surface of the E-glass/polyester unidirectional material is determined in the $G_I - G_{II} - G_{III}$ space.

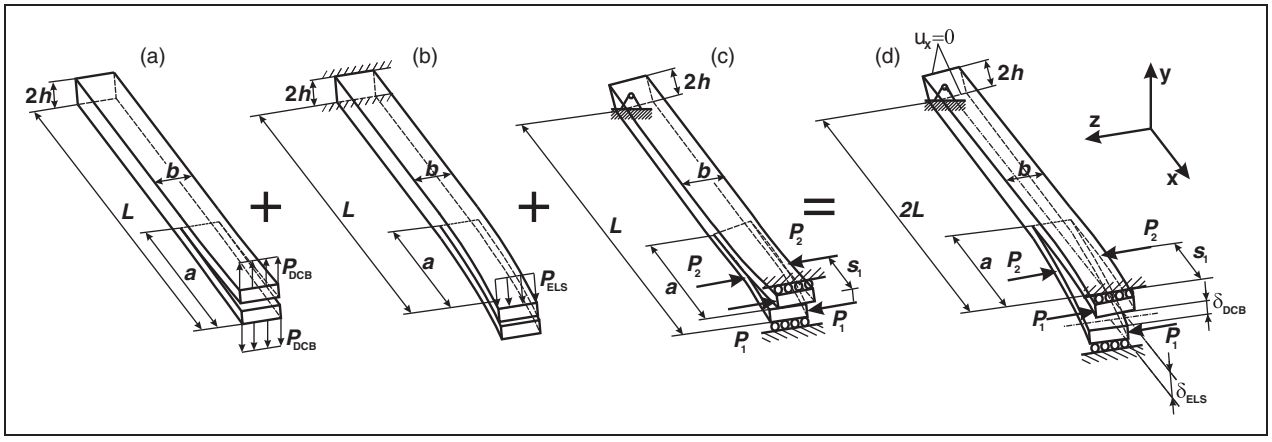

Figure 1. The prestressed split-cantilever beam ($PSCB_{I/II/III}$) specimen (d) as the superposition of the double-cantilever beam (DCB) (a), end-loaded split (ELS) (b) and MSCB (c) systems.

The PSCB specimen for mixed-mode I/II/III cracking

The $PSCB_{I/II/III}$ specimen is the combination of the DCB, ELS, and MSCB specimens. The 3D SOLIDWORKS model of the setup is demonstrated in Figure 2. The test method applies the rigs of the MSCB specimen, but the specimen is put into a prestresser, which is shown in Figure 3. To obtain mixed-mode I/II/III loading condition first we insert a steel roller (9) between the crack faces as a wedge. Second, the specimen is put into the notch (6) of the shaft (5) supported by ball (2) and roller bearings (4). Thanks to this latter fact, the specimen rotation is allowed. Although torsional deformation produces even mode-II effects, the specimen rotation can be prevented only by considerably stiff blocks leading to unwanted frictional effects.[20,22] The mode-II (ELS) loading is defined by a constant specimen end displacement through a set screw (7). It is important to note that neither the mode-I nor the mode-II related forces are measured, they can be determined only by an analytical or numerical model. Then, the doubly prestressed specimen is placed between the rigs of the MSCB setup in the way shown by Figure 4, where we can see the side, top and front views of the setup. The MSCB loading rigs transfer a scissor-like load to the prestressed specimen through rollers A and B. The external load, P_{MSCB}, is introduced through roller C by a testing machine. To ensure the position of rollers A and B along the thickness of the specimen, we applied set screws, which can be adjusted by using a screwdriver. This involves the rotation of the prestresser block about the z axis, as it is shown by the top view in Figure 4. The moment equilibrium of the system about the x axis is ensured by the shaft and the tube of the load transfer plate (refer to Figure 2). Essentially, we apply the virtual crack-closure technique (VCCT) for data reduction; however, to verify the load displacement-slopes and the linear elastic behavior of the system, the analytical compliance of the MSCB system is utilized.

Analysis

The analysis of the MSCB specimen is detailed in Ref. 27. The improved beam theory (IBT) model takes four mechanical deformations into account: bending and shearing of the specimen arms, the Saint-Venant effect at the crack front and the free torsion effect in the delaminated portion. The compliance and the ERR calculated by the analytical solution were compared to the results of a three-dimensional FE model and an excellent agreement was found. Since the MSCB specimen is loaded at four points, it should be mentioned that the compliance is calculated at the point of external load application, that is at roller C in Figure 4, apparently,

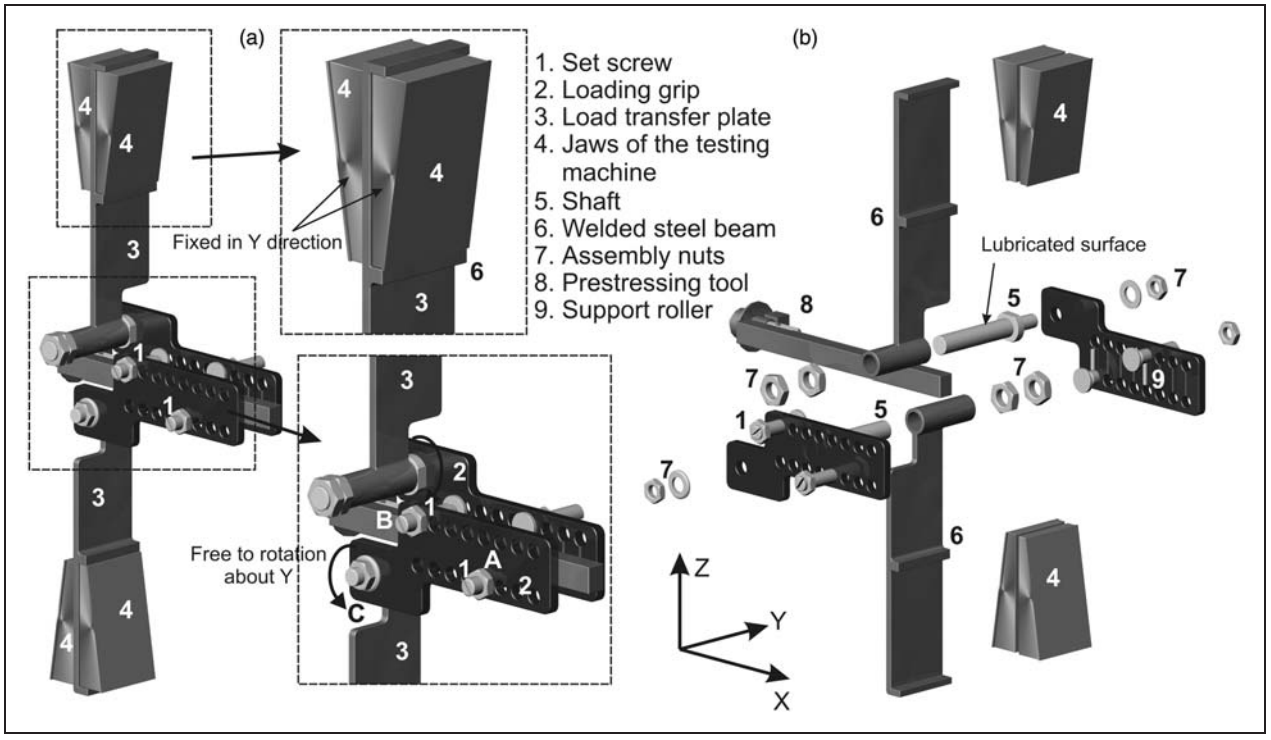

Figure 2. The 3D views of the prestressed split-cantilever beam ($PSCB_{I/II/III}$) specimen, assembled state (a), exploded view (b).

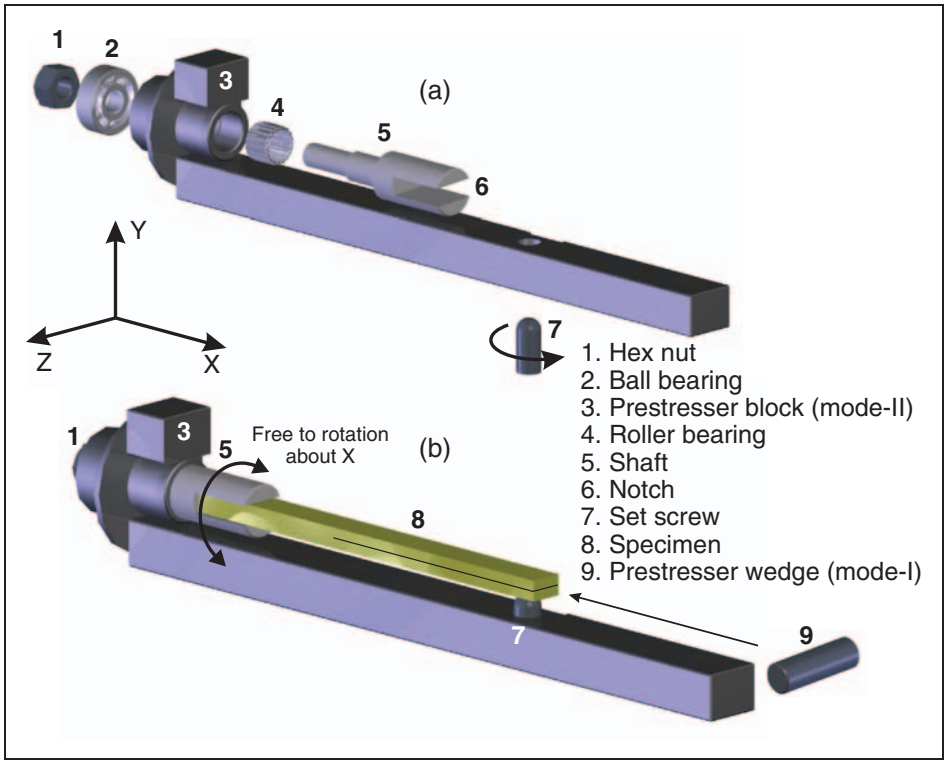

Figure 3. Prestresser for the prestressed split-cantilever beam ($PSCB_{I/II/III}$) specimen, assembled state (a), exploded view (b).

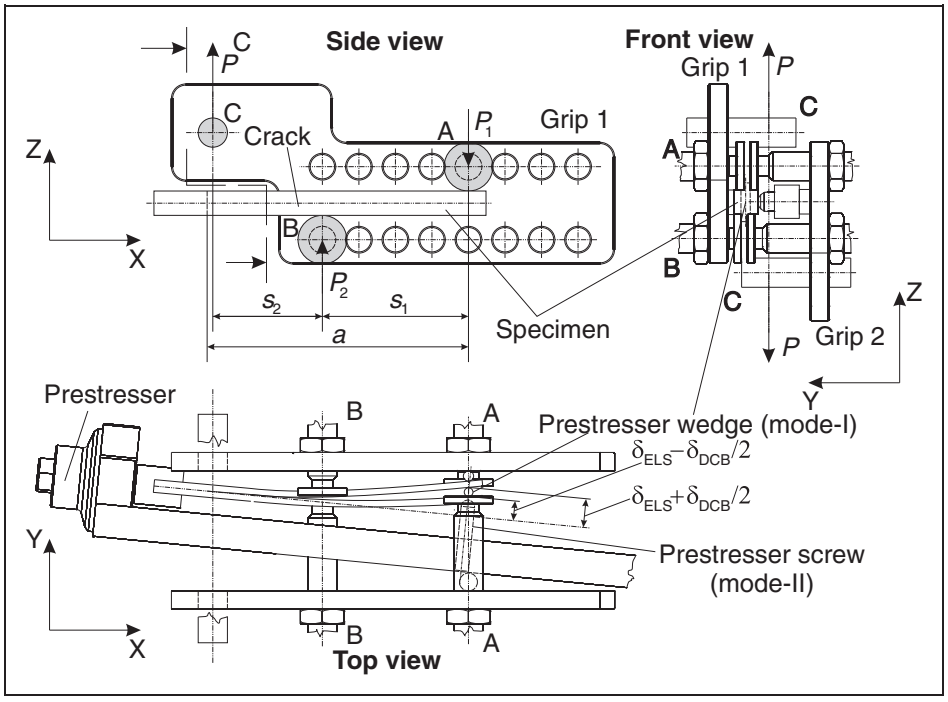

Figure 4. The side, front, and top views of the prestressed split-cantilever beam ($PSCB_{I/II/III}$) system.

the compliance can be measured only at this point, which is[27]:

$$C_{\mathrm{MSCB}} = \frac{8a^3}{b^3 h E_{11}}\left[f_{\mathrm{EB1}}^{\mathrm{MSCB}} + f_{\mathrm{TIM1}}^{\mathrm{MSCB}} + f_{\mathrm{FT1}}^{\mathrm{MSCB}} + f_{S-V1}^{\mathrm{MSCB}}\right], \tag{1}$$

where a is the crack length, b is the specimen width, h is the half specimen thickness, E_{11} is the flexural modulus. The terms in the brackets consider bending, transverse shear, free torsion, and Saint-Venant effect in the MSCB specimen:

$$f_{\mathrm{EB1}}^{\mathrm{MSCB}} = 1 - 3\left(\frac{s_1+s_2}{a}\right) + 3\left(\frac{s_1+s_2}{a}\right)^2 - \frac{s_1(s_1+s_2)(s_1+2s_2)}{a^3}, \tag{2}$$

$$f_{\mathrm{TIM1}}^{\mathrm{MSCB}} = 0.3\left(1 - \frac{s_2^2 - s_1^2}{a s_1}\right)\left(\frac{b}{a}\right)^2\left(\frac{E_{11}}{G_{13}}\right), \tag{3}$$

$$f_{\mathrm{FT1}}^{\mathrm{MSCB}} = 0.19\frac{1}{\varsigma}\left(1 - \frac{s_1}{a}\right)\left(\frac{b}{a}\right)^2\left(\frac{E_{11}}{G_{12}}\right), \tag{4}$$

$$f_{\mathrm{S-V1}}^{\mathrm{MSCB}} = 0.48\left(\frac{a-(s_1+s_2)}{a}\right)^2\left(\frac{b}{a}\right)\left(\frac{E_{11}}{G_{13}}\right)^{\frac{1}{2}}, \tag{5}$$

and:

$$\varsigma = 1 - 0.63\mu\frac{h}{b},\ \mu = \left(\frac{G_{13}}{G_{12}}\right)^{\frac{1}{2}}, \tag{6}$$

where G_{12} and G_{13} are the shear moduli in the x-y and x-z planes, respectively, s_1 and s_2 are the distances between the loading rollers A, B, and C, respectively (see Figure 4). The ERR can be calculated using the Irwin-Kies expression,[3] however, it gives a width-wise average value; therefore, it cannot be used in the $\mathrm{PSCB_{I/II/III}}$ system. It has been shown that the condition of at least a 96% mode-III dominant MSCB test is[27]:

$$1.02 \le a/(s_1+s_2) \le 1.09. \tag{7}$$

Equations (1) to (6) will be used to verify the linear elastic behavior of the system.

Energy release rate distributions

An important requirement against a mixed-mode setup is that the ERR distributions are uniform over the specimen width. In general, slight decays are expected at the edges. In the $\mathrm{PSCB_{I/II/III}}$ system it is shown that due to the complex stress state along the crack front, the ERR rate – and so the mode ratio – is strongly non-uniform.

In order to elaborate how the ERRs and the mode ratios change over the specimen width, we apply the ANSYS 12 package. The finite element model is shown by Figure 5. The elastic properties of the models were $E_{11} = 33$ GPa, $E_{22} = E_{33} = 7.2$ GPa, $G_{12} = G_{13} = G_{23} = 3$ GPa, and $\nu_{12} = \nu_{13} = \nu_{23} = 0.27$. The geometric properties were $b = 12.8$ mm, $2h = 6.2$ mm, $s_1 = 57.38$ mm, and $s_2 = 49.36$ mm and the length of the models was $L = 118$ mm (refer to Figure 1). We note that s_1 and s_2 were calculated based on a correction presented in Ref. 37. The imposed boundary conditions and the loading of the model are demonstrated in Figure 6. First, the model was loaded at the ends of the specimen arms by displacement values, δ_{ELS}-$\delta_{\mathrm{DCB}}/2$ and $\delta_{\mathrm{ELS}} + \delta_{\mathrm{DCB}}/2$, respectively, where the limit values of δ_{ELS} and δ_{DCB} were determined based on the pure mode-I DCB and mode-II ELS[38] tests. The prestressing provided the mode-I and mode-II parts of the mixed-mode I/II/III ERR. The mode-I displacement was equal to the roller diameter, the mode-II displacement values were calculated from the number of revolutions and the pitch (1.25 mm) of the prestressing screw. On the other hand, the model was also loaded in planes parallel to the delamination (from $h/2$ distance to the specimen side) applying the load values (P_1 and P_2), which were calculated using the experimentally measured P_{MSCB} loads based on crack initiation tests ($P_1 = P_{\mathrm{MSCB}} \cdot s_2/s_1$ and $P_2 = P_{\mathrm{MSCB}} \cdot (1 + s_2/s_1)$[27]). The ERRs were evaluated by using the VCCT (e.g. Ref. 39), the sizes of the crack tip elements were $\Delta x = \Delta y = 0.25$ mm and $\Delta z = 0.64$ mm. For the determination of G_{I}, G_{II}, and G_{III}, a so-called MACRO was written in the ANSYS Design and Parametric Language (ADPL). The MACRO gets the nodal forces and displacements at the crack tip and at each pair of nodes, respectively, then by defining the size of crack tip elements it determines and plots the ERRs at each point along the crack front.

Figure 7 shows the distribution of the ERRs along the crack front in the case of $\delta_{\mathrm{DCB}} = 6.0$ mm, $\delta_{\mathrm{ELS}} = 6.25$ mm and $\delta_{\mathrm{DCB}} = 12.0$ mm, $\delta_{\mathrm{ELS}} = 2.5$ mm. Based on the figures, we can see that the mode-II and mode-III ERRs are non-uniformly distributed over the specimen width. Moreover, only the mode-I ERR remains uniform, that is the same as that in a standard DCB specimen. Due to this variation in the ERR, constant mode ratios, namely $G_{\mathrm{I}}/G_{\mathrm{II}}$, $G_{\mathrm{I}}/G_{\mathrm{III}}$, and $G_{\mathrm{II}}/G_{\mathrm{III}}$, are not possible to be produced. Therefore, the ERR must be evaluated pointwise. It must be denoted that in our case, $s_1 + s_2 = 57.38 + 49.36 = 106.74$ mm, which violates Equation (7). That is because the position of the

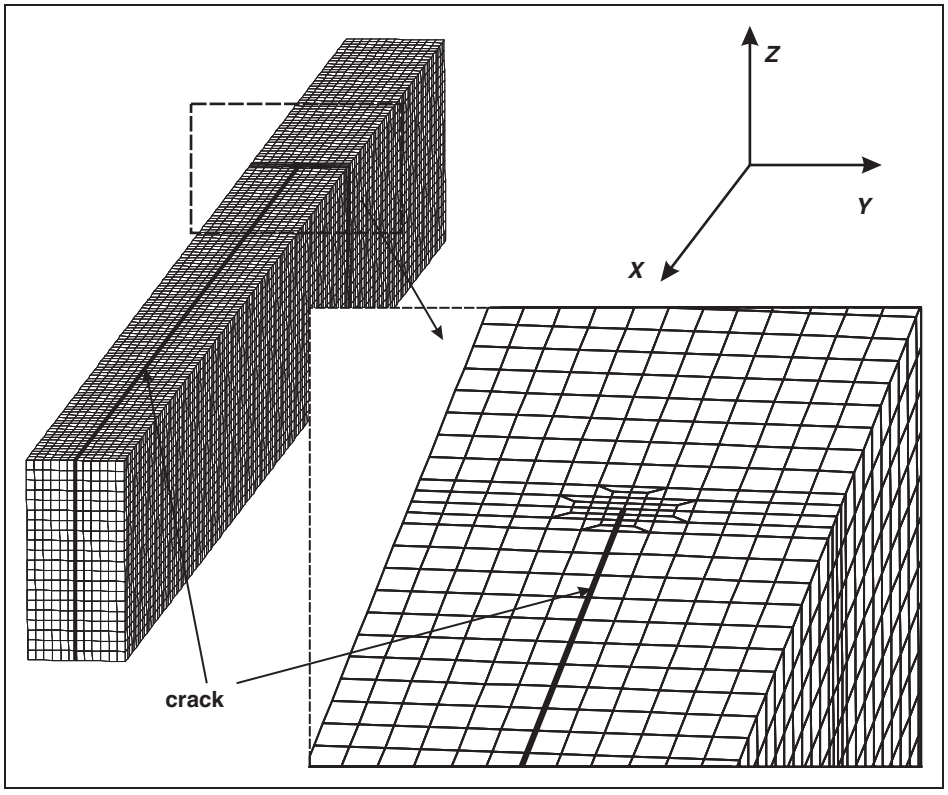

Figure 5. The ANSYS finite element model of prestressed split-cantilever beam ($PSCB_{I/II/III}$) specimen.

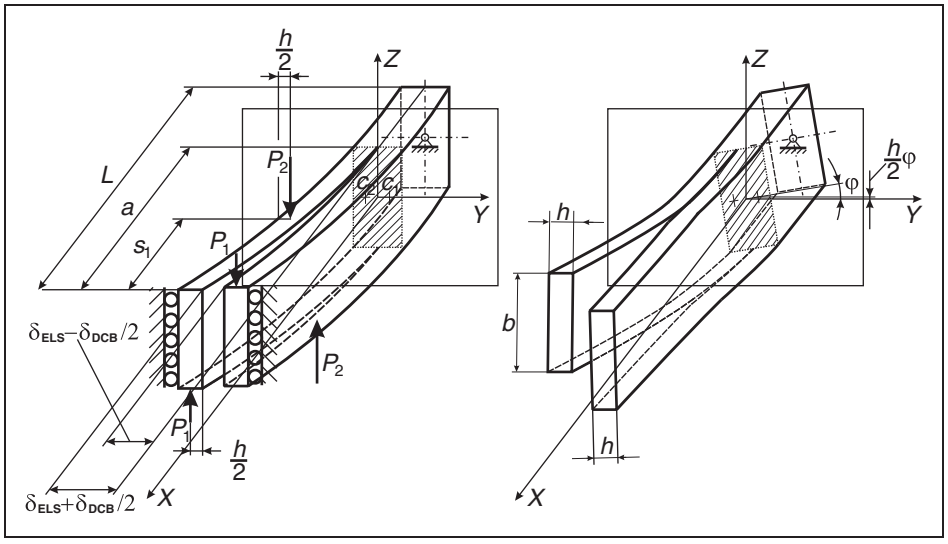

Figure 6. The applied kinematic and dynamic boundary conditions in the finite element model of the prestressed split-cantilever beam ($PSCB_{I/II/III}$) specimen.

loading screws of the rigs was fixed, and due to the given specimen width, we were not able to choose better positions for s_1 and s_2. Since the ERR varies along the crack front, the specimen possess a curved crack front under crack propagation.

Point of crack initiation

In the data reduction and calculation of the critical ERRs, it was assumed that the crack initiation takes place at the point where the highest value of the total

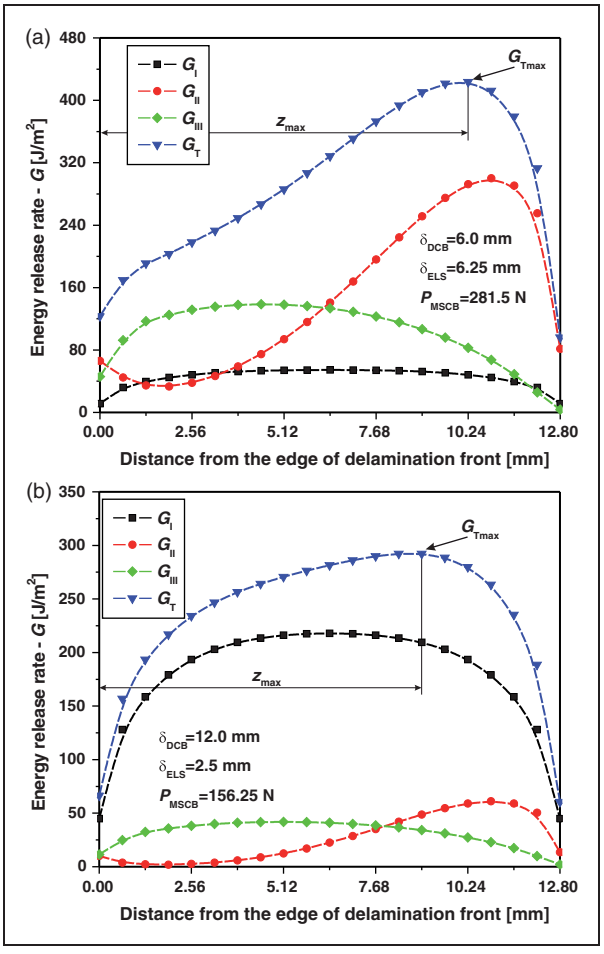

Figure 7. The distribution of the mode-I, mode-II, mode-III, and total energy release rates (ERRs) along the specimen width.

ERR ($G_T = G_I + G_{II} + G_{III}$) is available. This assumption will be validated later by experiments. It must be noted that the pointwise detection of crack initiation does not consider a significant volume of material, which is important for obtaining representative properties in heterogeneous materials. However, for mode-III testing, this is a significant difficulty. Based on the state-of-the-art, larger volume in general involves larger specimen dimensions, more than one crack initiation points,[26,31,32] and non-linear response.[13,29] The material volume considered in the $PSCB_{I/II/III}$ is relatively small, which is a drawback. On the other hand, the crack initiation can be detected accurately for transparent materials and the load-displacement response is linear.

Along the crack front of the specimen models the mode-I, mode-II, and mode-III ERRs are calculated by the VCCT and at each point the total ERR is determined. In the sequel, the details of the experimental work is presented.

Experiments

Material properties

The details of the specimen preparation and the determination of the material properties of the unidirectional E-glass/polyester composite material was presented in several other papers.[33,34] A quite important feature of the utilized glass/polyester specimens is the transparency, which makes it possible to follow the crack initiation visually, without any special equipment.

Double-cantilever beam test

The DCB (Figure 1(a)) test was performed previously in a past paper.[38] The width of the specimens was $b = 20$ mm, the crack length was $a = 105$ mm, and the measured data were evaluated by beam theory. In this work, we used the same data, however, the ERR is evaluated by the VCCT method. The finite element model of the specimen were created by ANSYS and $G_{IC} = 457 \pm 99$ J/m^2 was obtained in the midpoint of the crack front.

End-loaded split test

In the case of the ELS test (Figure 1(b)), we refer to previous fracture experiments[38] performed for $a = 105$ mm. Four specimens were tested and it has been found that the initation ERR was $G_{IIC} = 771 \pm 77$ J/m^2 evaluated by using the VCCT. Again, the initiation point was in the middle of the specimens.[38] The width of the specimens were $b = 20$ mm.

Modified split-cantilever beam test

For the MSCB (Figure 1(c)) measurements, four specimens were prepared with $a = 105$ mm, $b = 12.8$ mm, $s_1 = 49.25$ mm, and $s_2 = 51.15$ mm, respectively. Each specimen was put into the loading rig shown in Figure 2 (or detailed in Ref. 27), the rig was adjusted in order to eliminate any play of the specimens. Then the specimens were tested, the load and displacement values were read from the scale of the testing machine and using a digitronic indicator. The crack initiation was identified visually and when the first non-uniformity in the previously straight crack front was observed, it was believed to be the point of crack initiation (see Figure 8). We note that by keeping Equation (7), the MSCB test produces similar ERR ditribution to that of the DCB specimen, that is, initiation is expected in the midpoint over the specimen width.

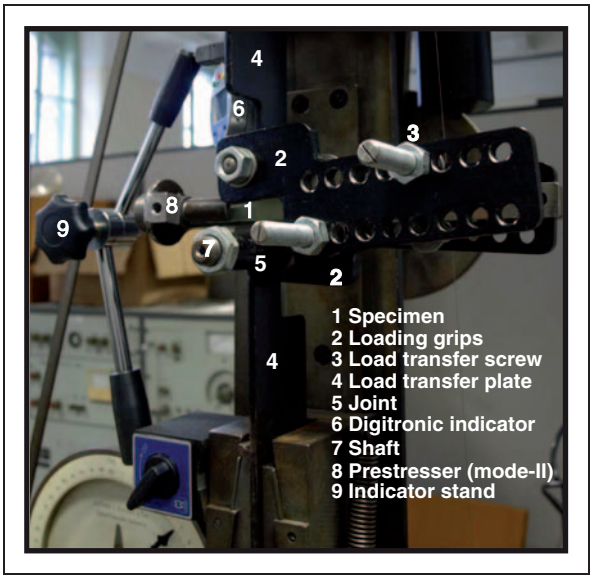

Figure 8. The experimental equipment for the prestressed split-cantilever beam ($PSCB_{I/II/III}$) system.

The initation ERR was $G_{IIIC} = 139 \pm 34\,J/m^2$, which took place at the midpoint of the crack front. This value is significantly less than G_{IC} and G_{IIC}, and in general the mode-III ERR is expected to be higher than G_{IC} and also G_{IIC}. It should be mentioned that in Ref. 30 for the same mateial, $G_{IIIC} = 446\,J/m^2$ was obtained. However, in the latter paper, the utilized MSCB fixture was not the same as the one shown in Figures 2 and 8. The rigs were connected to each other by screws, which induced friction between them. Probably, this effect caused the mentioned difference. On the other hand, the crack length of interest was $a = 55$ mm in Ref. 30, in contrast with the current tests, where we applied specimens with $a = 105$ mm. A certain dependence on the crack length can exist.[37] In general, the mode-III toughness for glass fiber-reinforced composites reported in the literature is much higher[14,40,41] (1200-3000 J/m^2) than the value obtained in this paper. Nevertheless, the former works presented ECT test results with multidirectional lay-ups, while the present test applied unidirectional beam-like samples.

Mixed-mode I/II prestressed end-loaded split test

The $PELS_{I/II}$ test was presented in Ref. 38. This test is the combination of the DCB and ELS systems, where the DCB part was preloaded by steel rollers, the ELS part was provided by the load introductor of a testing machine. The crack length of interest was $a = 105$ mm. The critical crack opening displacement measured from the DCB test[38] is about 15 mm (if $a = 105$ mm). Six steel rollers were used including the following diameters: $d_0 = 6$, 7, 8, 10, 12, and 13 mm. It was assumed that the δ_{DCB} values were identical to these diameters. The specimen arms transmitted a relatively high pressure to the steel roller, therefore the position of the rollers was always stable and no slip along the x axis was observed during the measurements. Similarly to the ELS tests, we applied four coupons at each steel roller. The load-deflection data was measured by using the scale of the testing machine and a digitronic indicator. In each case, the critical load at crack initiation was determined.

Mixed-mode I/III prestressed split-cantilever beam test

The $PSCB_{I/III}$ test is detailed in Ref. 33. Apparently, this test is based on the DCB + MSCB combination. The crack length of interest was $a = 105$ mm, the the width of the specimens was $b = 12.4$ mm. Six steel rollers were used, the same as those of the $PELS_{I/II}$ test. Similarly to the MSCB tests, we applied four coupons at each steel roller. The load-deflection data was measured by using the scale of the testing machine and a mechanical dial gauge. In each case, the critical load at crack initiation was determined.

Mixed-mode II/III prestressed split-cantilever beam test

The $PSCB_{II/III}$ test setup was recently introduced in Ref. 35. The test is the superposition of the ELS and MSCB configurations. The crack length of interest was $a = 105$ mm, the width of the specimens was $b = 12.8$ mm. The critical specimen end displacement measured from the ELS test[38] is about 14 mm (if $a = 105$ mm and $L = 118$ mm). According to this fact, six different values of the ELS displacement δ_{ELS} were set: 4.6875, 6.25, 8.125, 9.375, 10.625, and 11.875 mm. This step was done by touching the specimen surface first, then by knowing the pitch of the prestresser screw the δ_{ELS} displacement was set. Afterward, the prestresed specimen was placed between the MSCB rigs. The setup and the concept of the system is in fact the same as that of the $PSCB_{I/II/III}$ (Figure 2), but the mode-I prestressing does not apply. Similarly to the MSCB tests, we applied four coupons at each displacement value. The load-deflection data was measured by using the scale of the testing machine and a digitronic indicator. In each case, the critical load (P_{MSCB}) at crack initiation was determined.

Mixed-mode I/II/III prestressed split-cantilever beam test

This test combines the DCB, ELS, and MSCB systems. As it has already been shown in Figure 2, a double prestressing method is applied. The mode-I ERR is

provided by a steel roller, while the mode-II ERR is given by the prestresser detailed in Figure 3. Thus, using the MSCB rigs it is possible to induce mixed-mode I/II/III conditions. The experimental equipment is shown in Figure 8. Essentially, the same concept was applied as in the previous prestressed specimens. By setting the mode-I and mode-II displacements, it is possible to cover the whole $G_I - G_{II} - G_{III}$ space. Eventually, we need to know the critical crack opening and crack sliding displacements of the DCB and ELS tests, respectively. These are known from the DCB and ELS measurements.[38] The δ_{DCB} and δ_{ELS} pairs applied in the $PSCB_{I/II/III}$ test were determined based on the $PELS_{I/II/}$, $PSCB_{I//III}$, and $PSCB_{II/III}$ data using

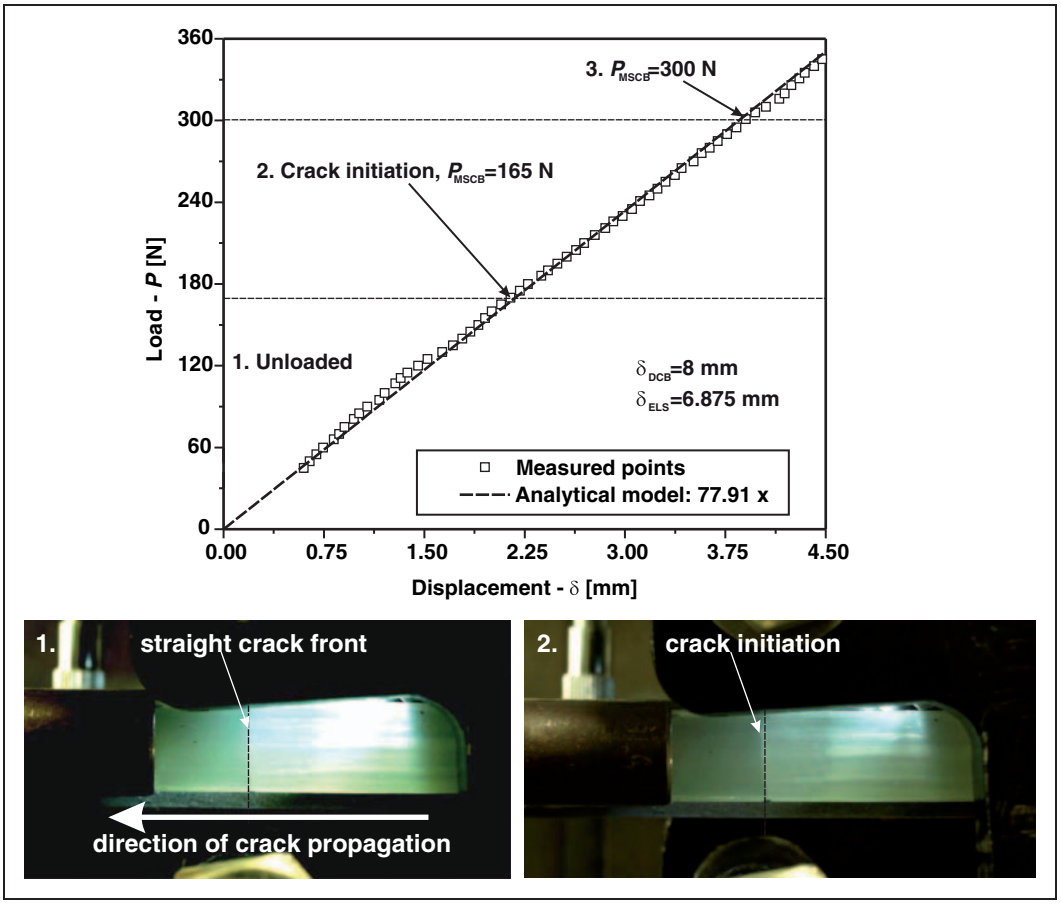

Figure 9. The load-displacement curve of the prestressed split-cantilever beam ($PSCB_{I/II/III}$) specimen for $\delta_{DCB} = 8.0$ mm, $\delta_{ELS} = 6.875$ mm (a). The identification of crack initiation during the fracture process (b).

Table 1. The influence of double prestressing on the load-displacement slopes of the $PSCB_{I/II/III}$ system

δ_{DCB} (mm)	δ_{ELS} (mm)	Slope-1 (N/mm)	Difference (%)[a]	Slope-2 (N/mm)	Difference (%)[a]
6	4.6875	77.8	0.2	76.7	1.6
7	6.875	73.1	6.6	75.6	3.1
8	5.625	74.7	4.3	76.9	1.4
10	3.4375	80.4	−3.1	75.4	3.4
12	2.5	78.4	−0.6	76.2	2.2
13	2.1875	76.1	2.3	74.4	4.8

[a]DCB: double-cantilever beam. Difference compared to the analytical model, Equation (1) (77.91 N/mm).

Table 2. Energy release rates (ERRs) data in the $G_I - G_{II} - G_{III}$ space

Config.	δ_{DCB} (mm)	δ_{ELS}(mm)	P_{MSCB}(N)	z_{max}(mm)	G_I (J/m^2)	G_{II} (J/m^2)	G_{III} (J/m^2)	G_T (J/m^2)
MSCB[a]	0	0	247.8	6.4	0	0	139 ± 34	139
$PSCB_{II/III}$	0	4.6875	338.8	10.24	0	234 ± 8	132 ± 11	366
	0	6.25	329.0	10.24	0	325 ± 6	117 ± 6	442
	0	8.125	311.5	10.24	0	448 ± 12	97 ± 10	546
	0	9.375	297.5	10.24	0	540 ± 15	83 ± 11	623
	0	10.625	286.3	10.24	0	642 ± 11	71 ± 7	713
	0	11.875	211.8	10.24	0	687 ± 19	30 ± 8	718
$PSCB_{I/III}$	6	0	226.5	7.8125	48	0	131 ± 9	179
$PSCB_{I/II/III}$	6	3.125	305.5	9.6	51	124 ± 4	125 ± 9	300
	6	4.6875	293.0	10.24	48	208 ± 17	97 ± 21	353
	6	6.25	281.5	10.24	48	293 ± 24	83 ± 23	424
	6	8.125	267.8	10.24	48	413 ± 8	68 ± 6	530
	6	10.3125	201.0	10.24	48	534 ± 18	29 ± 8	611
$PELS_{I/II}$	6	16.1	-	10	54	534 ± 58	0	588
$PSCB_{I/III}$	7	0	214.0	7.8125	65	0	123 ± 14	187
$PSCB_{I/II/III}$	7	2.5	273.8	9.6	69	89 ± 6	101 ± 15	259
	7	4.6825	256.5	9.6	69	175 ± 7	82 ± 10	326
	7	5.625	245.5	10.24	66	229 ± 13	65 ± 15	360
	7	6.875	204.0	10.24	66	281 ± 12	38 ± 8	385
	7	8.4375	136.8	9.6	69	333 ± 37	15 ± 5	417
$PELS_{I/II}$	7	12.8	-	6.4	73	338 ± 49	0	410
$PSCB_{I/III}$	8	0	193.0	7.8125	85	0	95 ± 9	180
$PSCB_{I/II/III}$	8	1.875	257.5	9.6	90	64 ± 1	91 ± 4	245
	8	3.125	231.5	9.6	90	97 ± 5	70 ± 8	257
	8	5	220.5	9.6	90	173 ± 2	57 ± 2	320
	8	5.625	198.0	9.6	90	195 ± 6	45 ± 6	330
	8	6.875	156.3	9.6	90	243 ± 8	24 ± 5	358
$PELS_{I/II}$	8	11.0	-	6.4	96	249 ± 48	0	345
$PSCB_{I/III}$	10	0	171.6	8.59375	133	0	74 ± 7	207
$PSCB_{I/II/III}$	10	2.1875	215.0	8.96	145	52 ± 1	67 ± 5	265
	10	3.4375	220.0	9.6	141	105 ± 8	62 ± 13	308
	10	4.6875	170.0	9.6	141	138 ± 3	33 ± 2	311
$PELS_{I/II}$	10	8.8	-	6.4	149	160 ± 42	0	310
$PSCB_{I/III}$	12		133.0	9.375	192	0	40 ± 3	232
$PSCB_{I/II/III}$	12	1.25	158.0	8.32	214	17 ± 1	39 ± 3	269
	12	2.5	156.3	8.96	209	45 ± 8	35 ± 2	294
$PELS_{I/II}$	12	5.6	-	6.4	215	63 ± 15	0	279
$PSCB_{I/III}$	13		115.3	8.59375	227	0	32 ± 2	259
$PSCB_{I/II/III}$	13	2.1875	113.7	8.32	251	27 ± 4	20 ± 1	300
$PELS_{I/II}$	13	4.2	-	6.4	253	36 ± 8	0	288
DCB[b]	~15	-	-	6.4	457 ± 99	0	0	457
ELS[b]	0	19.4	-	6.4	0	771 ± 77	0	771

[a]DCB: double-cantilever beam, ELS: end-loaded split. $s_1 = 49.25$ mm, $s_2 = 51.15$ mm.
[b]$b = 20$ mm.

improved beam theory (IBT) models, which were presented in.[33,35,38] During the tests for each pair of δ_{DCB} and δ_{ELS}, four specimens were tested, the critical load at crack initiation (P_{MSCB}) was recorded, as well as the displacement values. The crack initiation was identified visually, at some points the crack front as well as the sign of crack initiation was photographed.

Results and discussion

It will be shown subsequently that the stiffness, the compliance, and the mode-III ERR of the $PSCB_{I/II/III}$ specimen are identical to those of the MSCB specimen.

Load and displacement

Figure 9(a) shows a recorded load-displacement trace for the $PSCB_{I/II/III}$ specimen if $\delta_{DCB} = 8.0\,mm$ and $\delta_{ELS} = 6.875\,mm$. The response follows essentially a linear relation. The $PSCB_{I/II/III}$ test was performed according to the followings. The onset of crack advance was identified by visual observations. In each case, four specimens were tested, one of them was used to investigate the crack front. Accordingly, the former specimen was loaded subsequently. When the first non-uniformity was observed, then this point was denoted to be the point of fracture initiation. The results of this process are demonstrated in Figure 9(b) for the $PSCB_{I/II/III}$ system at a prestressed state with $\delta_{DCB} = 8.0\,mm$ $\delta_{ELS} = 6.875\,mm$. Also, the crack initiation point in Figure 9(b) agrees quite well with the G_{Tmax} point indicated in Figure 7. The dashed line in Figure 9(a) shows the result of Equation (1), indicating the accuracy of the analytical compliance. Table 1 shows that there are only insignificant differences between the slopes of the load-displacement traces of the MSCB ($\delta_{DCB} = 0$, $\delta_{ELS} = 0$, analytical model) and $PSCB_{I/II/III}$ specimens, consequently the prestressed state does not influence noticeably the stiffness of the system and the compliance of the $PSCB_{I/II/III}$ can be assumed to be equal to that of the MSCB system. The maximum difference is 4.8% between the measured and calculated slopes.

Critical energy release rates

Table 2 presents the critical mode-I, mode-II, and mode-III ERRs at crack initiation calculated by the VCCT method. At each value of the prestress displacements (δ_{DCB} and δ_{ELS}), four coupons were used. Table 2 covers the measured data including the DCB, ELS, MSCB and the $PELS_{I/II}$, $PSCB_{I/III}$, $PSCB_{II/III}$ as well as the $PSCB_{I/II/III}$ specimens. In each case, the position where we can expect crack initiation is indicated (z_{max}). In the $PSCB_{I/II/III}$ test this point varies slightly. On the other hand in the pure mode tests it is always the midpoint, where the highest total ERR takes place. The scatter of the ERR is also included in Table 2. The scatter of the mode-I ERR is zero due to the prestressing. Although the ELS part is also provided by prestressing, even the MSCB part induces mode-II.

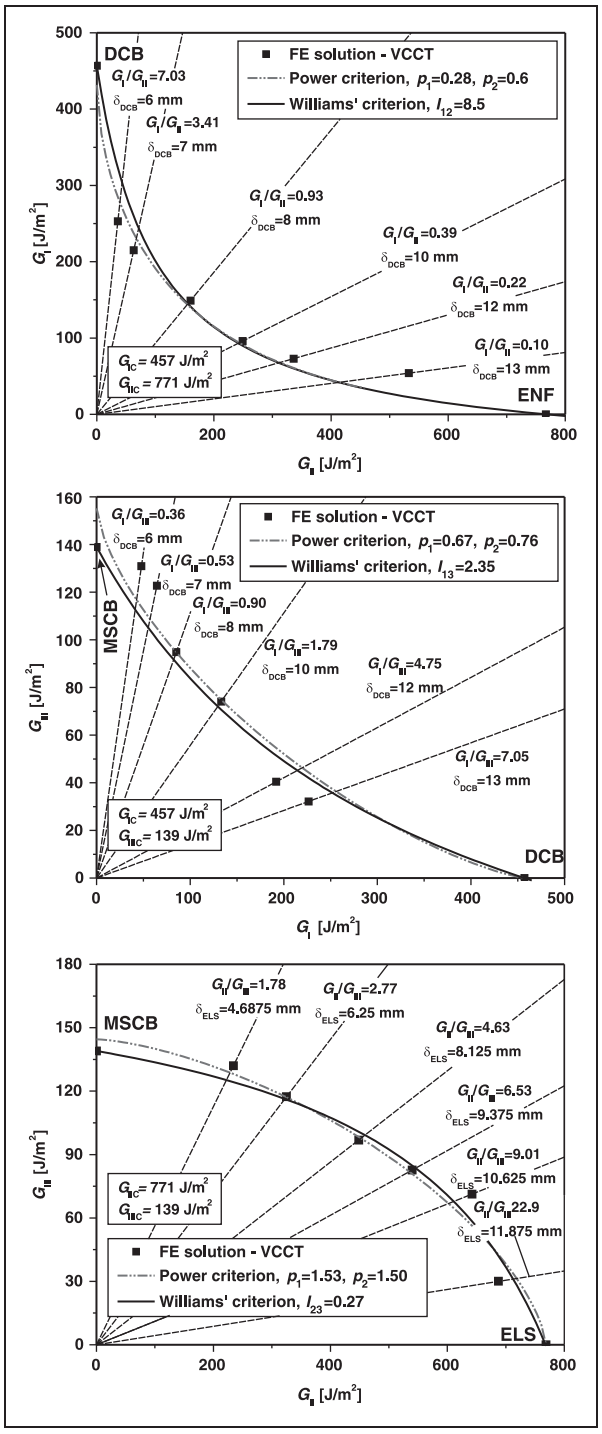

Figure 10. Interlaminar fracture envelopes in the $G_I - G_{II}$ (a), $G_I - G_{III}$ (b), and $G_{II} - G_{III}$ (c) planes for glass/polyester unidirectional composite.

Table 3. Results of the fracture criterion (Equation (9)) at the points of the crack front for the $PSCB_{II/III}$ specimen, $\delta_{ELS} = 9.375$ mm, $P_{MSCB} = 297.5$ N

z – distance from the edge of delamination front [mm]	0.00	1.28	2.56	3.84	5.12	6.40	7.68	8.96	10.24	11.52	12.80
Criterion – Equation (9)	0.62	1.12	1.18	1.20	1.19	1.16	1.12	1.07	0.99[a]	0.84	0.24

[a]ELS: end-loaded split. Point of crack initiation.

Therefore, the scatter of the mode-II ERR is listed in Table 2, but it does not represent the realistic values. Finally, the scatter of the mode-III ERRs is within reasonable ranges.

Fracture envelopes and fracture surface

In order to construct a fracture surface in the $G_I - G_{II} - G_{III}$ space, first we need the envelopes in the $G_I - G_{II}$, $G_I - G_{III}$, and $G_{II} - G_{III}$ planes, which have already been determined in previous works using two criteria.[33,35,38] In accordance with the traditional power criterion, the following relation may be established between the ERRs[42,43]:

$$\left(\frac{G_i}{G_{iC}}\right)^{p_1} + \left(\frac{G_j}{G_{jC}}\right)^{p_2} = 1, \tag{8}$$

where $i = \text{I, II, III}$, $j = \text{I, II, III}$, and $i \neq j$. Williams' criterion[42,43] recommends the following expression for the relation between the ERRs:

$$\frac{G_i}{G_{iC}} + \frac{G_j}{G_{jC}} + (I_{kl} - 1)\left(\frac{G_i}{G_{iC}}\right)\left(\frac{G_j}{G_{jC}}\right) = 1, \tag{9}$$

where I_{kl} is the interaction parameter between the mode-i and mode-j ERRs, moreover $k = 1,2,3$, $l = 1,2,3$, and $k \neq l$, and finally if $i = \text{I}$ then $k = 1$, etc. If $I_{kl} = 0$, then there is no interaction. Also, if $I_{kl} = 1$, then Equation (9) states a simple addition. In Equations (8) and (9), G_{iC} and G_{jC} are the critical ERR under pure mode-i and mode-j (calculated from the data of the DCB, ELS, or MSCB specimens, respectively). The results of the $PELS_{I/II}$, $PSCB_{I/III}$, and $PSCB_{II/III}$ tests listed in Table 2 were used to provide additional points in the $G_i - G_j$ planes. The power parameters (p_1, p_2) in Equation (8) and the interaction parameter (I_{ij}) in Equation (9) were determined by a non-linear curve-fit technique applying the ORIGINPRO 7.0 code.

The fracture envelopes calculated by the VCCT method are displayed in Figure 10. As it can be seen, there are significant interactions between the different fracture modes. Also, the material behaves similarly under mixed-mode I/II and I/III conditions but proves a completely different behavior under mixed-mode II/III conditions. Overall, the difference between the power and Williams' criteria is negligible; both describe the same failure locus. The fracture surface of the tested material can be determined by using the data of the $PSCB_{I/II/III}$ test. To fit the reduced data, the following surface equation was applied:

$$\begin{aligned}\frac{G_I G_{II}}{G_{IC} G_{IIC}}(I_{12} - 1) + \frac{G_{II} G_{III}}{G_{IIC} G_{IIIC}}(I_{23} - 1) \\ + \frac{G_I G_{III}}{G_{IC} G_{IIIC}}(I_{13} - 1) + \frac{G_I G_{II} G_{III}}{G_{IC} G_{IIC} G_{IIIC}} I_{123} \\ + \left(\frac{G_I}{G_{IC}} + \frac{G_{II}}{G_{IIC}} + \frac{G_{III}}{G_{IIIC}}\right) = 1,\end{aligned} \tag{10}$$

which is in fact the generalization of Williams' criterion for the 3D case. The interaction parameters I_{12}, I_{13}, and I_{23} are determined based on the $PELS_{I/II}$, $PSCB_{I/III}$, and $PSCB_{II/III}$ tests. The parameter, I_{123}, can be obtained by fitting the mixed-mode I/II/III ERR data. Equation (9) can be recovered from Equation (10) by setting one of the ERRs to zero. It is important to note that by knowing the critical ERRs (G_{IC}, G_{IIC}, G_{IIIC}) and the interaction parameters (I_{12}, I_{13}, I_{23} and I_{123}), it is possible to apply Equations (9) and (10) in the other points along the crack front. As Table 3 shows, in this case it is possible that we obtain a number higher than unity in the right-hand side of Equations (9) and (10), which means seemingly that there are more dangerous points apart from the point of crack initiation. However, it is important that Equations (9) and (10) assume crack initiation, which was detected only at one point, namely, where G_T was maximal (refer to Figure 7). Therefore, the other points, where Equations (9) and (10) gives >1, should be ignored.

The measured points in the $G_I - G_{II} - G_{III}$ space are shown in Figure 11(a), the fracture surface is presented in Figure 11(b). The spatial interaction parameter was $I_{123} = -8.23$, indicating significant interaction among the fracture modes.

Conclusions

In this work, the mixed-mode I/II/III version of the prestressed split-cantilever specimen was developed for interlaminar fracture testing of laminated transparent composite materials. Apart from the DCB, ELS, MSCB, $PELS_{I/II}$, $PSCB_{I/III}$, and $PSCB_{II/III}$ systems, the $PSCB_{I/II/III}$ specimen was used to obtain the

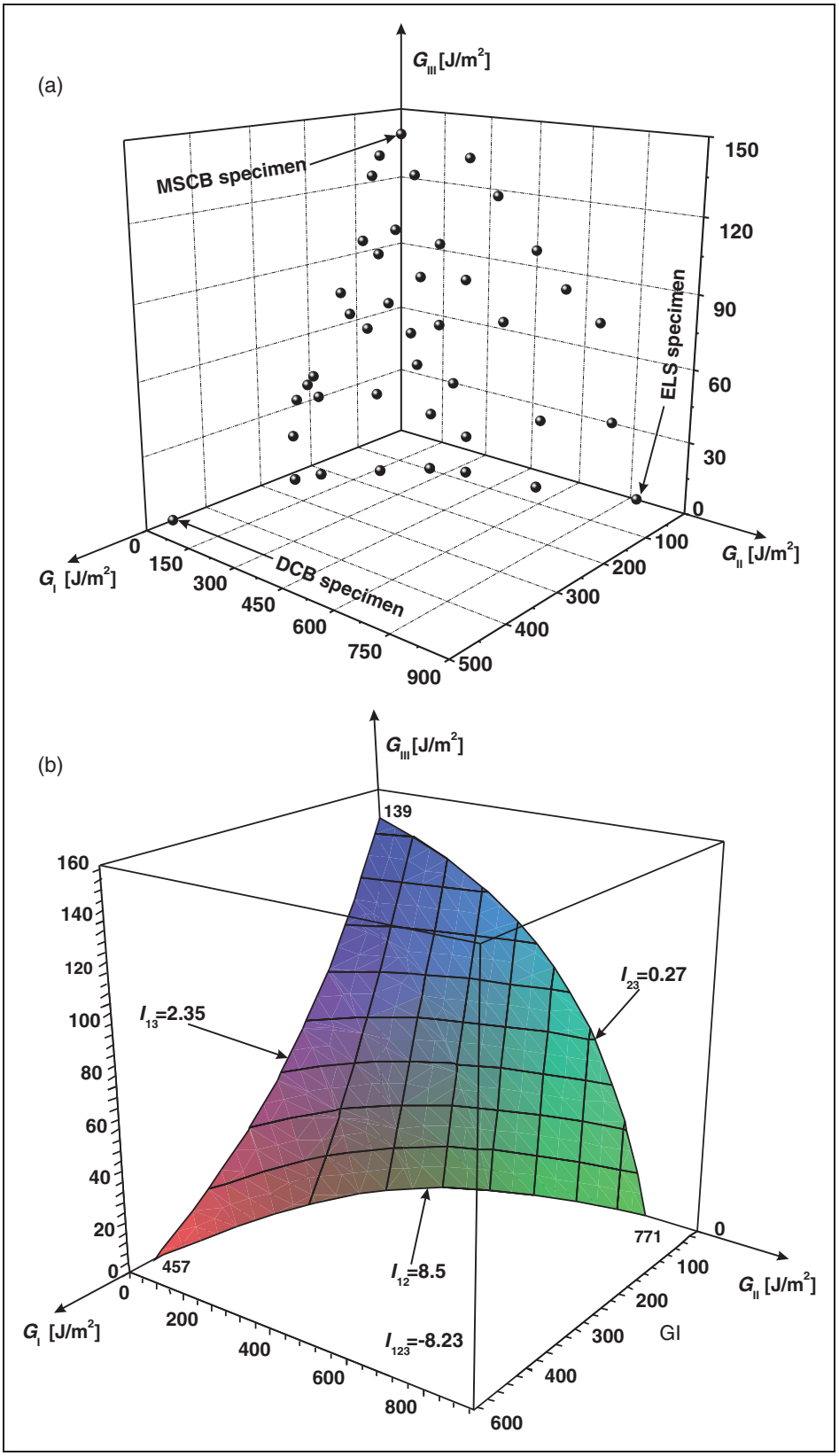

Figure 11. Interlaminar fracture surface in the $G_I - G_{II} - G_{III}$ space for glass/polyester unidirectional composite.

mixed-mode I/II/III energy release rate at crack propagation onset. To perform the experiments unidirectional E-glass/polyester specimens were manufactured and tested. The measured data was reduced by the VCCT method and it was shown that the mode ratio changes along the specimen width and it is not possible to eliminate this variation. Based on the experimental observations and energy release rate distributions, the crack initiation took place at the point where the highest total energy release rate was obtained. By producing mixed-mode I/II/III fracture conditions, the fracture surface of the present material was determined, indicating a significant interaction among G_I, G_{II}, and G_{III}.

Although an effective mode-III fracture test has not yet been developed, in this work the MSCB specimen was extended for mixed-mode I/II/III delamination testing of composites. The $PSCB_{I/II/III}$ specimen offers several advantages. First, it incorporates the traditional beam-like specimen geometry. Second, it was shown that the $PSCB_{I/II/III}$ specimen is able to produce any mode ratio at crack propagation onset. The drawbacks of the $PSCB_{I/II/III}$ specimen are that the mode ratio changes with the crack length and the applied load, so the method is recommended mainly for the testing of transparent composite materials. Moreover, the mode ratios changes along the crack front too. Due to this significant change, the ERRs must be evaluated pointwise along the crack front. Finally, the mode ratios cannot be calculated without performing experiments (i.e. they cannot be designated before the test), involving the fact that the mode ratios will depend on the definition of the crack initiation and the accuracy of the measurement of the load and crack length.

More research is required to reduce the drawbacks of the test and to make it possible to test non-transparent materials as well as for specimens with different lay-ups.

Acknowledgments

This work is connected to the scientific program of the 'Development of quality-oriented and harmonized R + D + I strategy and functional model at BME' project. This project is supported by the New Hungary Development Plan (Project ID: TÁMOP - 4.2.1/B-09/1/KMR-2010-0002). The first author is grateful to his father (András L. Szekrényes) for the construction of the experimental equipment.

Funding

This work was supported by the János Bolyai Research Scolarship of the Hungarian Academy of Sciences and the Hungarian Science and Research Fund (OTKA) [grant number T34040 (69096)].

References

1. Brunner AJ and Flüeler P. Prospects in fracture mechanics of 'engineering' laminates. *Eng Fract Mech* 2005; 72: 899–908.
2. Brunner AJ, Blackman BRK and Davies P. A status report on delamination resistance testing of polymer–matrix composites. *Eng Fract Mech* 2008; 75: 2779–2794.
3. Anderson TL. *Fracture mechanics – fundamentals and applications*, 3rd ed. Boca Raton, London, New York, Singapore: CRC Press, Taylor & Francis Group, 2005.
4. O'Brien TK and Raju IS. Strain energy release rate analysis of delamination around an open hole in composite materials. In: *25th AIAA/ASME/ASCE/AHS Structures, Structural Dynamics and Materials Conference*, Palm Springs, CA, 1984, pp.526–536.
5. Ge D, Liu F and Lu M. Effect of mode III fracture on composite laminates. *Compos Struct* 2004; 63: 469–480.
6. Becht G and Gillespie Jr JW. Design and analysis of the crack rail shear specimen for mode III interlaminar fracture. *Compos Sci Technol* 1988; 31: 143–157.
7. Donaldson SL. Mode III intelaminar fracture characterization of composite materials. *Compos Sci Technol* 1988; 32: 225–249.
8. Hwang S-F and Hu C-L. Tearing mode interlaminar fracture toughness of composite materials. *Polymer Compos* 2001; 22: 57–64.
9. Naik NK, Reddy KS, Meduri S, Raju NB, Prasad PD, Azad SKNM, et al. Interlaminar fracture characterization for plain weave fabric composites. *J Mater Sci* 2002; 37: 2983–2987.
10. Lee SM. An edge crack torsion method for mode III delamination fracture testing. *J Compos Technol Res* 1993; 15: 193–201.
11. Liao WC and Sun CT. The determination of mode III fracture toughness in thick composite laminates. *Compos Sci Technol* 1996; 56: 489–499.
12. Suemasu H. An experimental method to measure the mode-III interlaminar fracture toughness of composite materials. *Compos Sci Technol* 1999; 59: 1015–1021.
13. Ratcliffe JG. Characterization of the edge crack torsion (ECT) test for mode III fracture toughness measurement of laminated composites. *NASA/Technical Memorandum* 2004; 213–269.
14. Pennas D, Cantwell WJ and Compston P. The influence of strain rate on the mode III interlaminar fracture of composite materials. *J Compos Mater* 2007; 41: 2595–2614.
15. de Morais AB, Pereira AB, de Moura MFSF and Magalhães AG. Mode III interlaminar fracture of carbon/epoxy laminates using the edge crack torsion (ECT) test. *Compos Sci Technol* 2009; 69: 670–676.
16. de Moura MFSF, Fernandez MVC, de Morais AB and Campilho RDSG. Numerical analysis of the Edge Crack Torsion test for mode III interlaminar fracture of composite laminates. *Eng Fract Mech* 2008; 76: 469–478.
17. Adams DF, Carlsson LA and Pipes RB. *Experimental characterization of advanced composite materials*, 3rd ed. Boca Raton, London, New York, Washington: CRC Press, 2003.

18. Robinson P and Song QD. The development of an improved mode III delamination test for composites. *Compos Sci Technol* 1994; 52: 217–233.
19. Cicci D, Sharif F and Kortschot MT. Data reduction for the split cantilever beam mode III delamination test. In: *Proceedings, ACCM 10*, Whistler, British Columbia, Canada, 14–18 August, 1995.
20. Sharif F, Kortschot MT and Martin RH. Mode III Delamination Using a Split Cantilever Beam. In: Martin RH, *Composite materials: fatigue and fracture*. 5th Vol. ASTM STP 1230, 1995 ed. Philadelphia: ASTM, 85–99.
21. Trakas K and Kortschot MT. The relationship between critical strain energy release rate and fracture mode in multidirectional carbon-fiber/epoxy laminates. In: Armanios EA (ed.) *Composite materials: fatigue and fracture*. 6th Vol. ASTM STP 1285, 1997, ASTM, 283–304.
22. Rizov V, Shindo Y, Horiguchi K and Narita F. Mode III interlaminar fracture behaviour of glass fiber reinforced polymer woven laminates at 293 to 4 K. *Appl Compos Mater* 2006; 13: 287–304.
23. Farshad M and Flüeler P. Investigation of mode III fracture toughness using an anti-clastic plate bending method. *Eng Fract Mech* 1998; 60: 5–6.
24. Podczeck F. The determination of fracture mechanics properties of pharmaceutical materials in mode III loading using an anti-clastic plate bending method. *Int J Pharmaceutics* 2001; 227: 39–46.
25. Yoshihara H. Examination of the 4-ENF test for measuring the mode III R-curve of wood. *Eng Fract Mech* 2006; 73: 42–63.
26. de Morais AB and Pereira AB. Mode III interlaminar fracture of carbon/epoxy laminates using a four-point bending plate test. *Compos Appl Sci Manuf* 2009; 40: 1741–1746.
27. Szekrényes A. Improved analysis of the modified split-cantilever beam for mode-III fracture. *Int J Mech Sci* 2009; 51: 682–693.
28. Pereira AB, de Morais AB and de Moura MFSF. Design and analysis of a new six point edge crack torsion (6ECT) specimen for mode III interlaminar fracture characterisation. *Compos Appl Sci Manuf* 2011; 42: 131–139.
29. Davidson BD and Sediles FO. Mixed-mode I-II-III delamination toughness determination via a shear-torsion-bending test. *ComposAppl Sci Manuf* 2011; 42: 589–603.
30. Szekrényes A. Delamination fracture analysis in the G_{II}-G_{III} plane using prestressed transparent composite beams. *Int J Solids Struct* 2007; 44: 3359–3378.
31. Pereira AB and de Morais AB. Mixed mode I + III interlaminar fracture of carbon/epoxy laminates. *Compos Appl Sci Manuf* 2009; 40: 518–523.
32. de Morais AB and Pereira AB. Mixed mode II + III interlaminar fracture of carbon/epoxy laminates. *Compos Sci Technol* 2008; 68: 2022–2027.
33. Szekrényes A. Interlaminar fracture analysis in the G_{I}-G_{III} plane using prestressed composite beams. *Compos Appl Sci Manuf* 2009; 40: 1621–1631.
34. Suemasu H, Kondo A, Gozu K and Aoki Y. Novel test method for mixed mode II and III interlaminar fracture toughness. *Adv Compos Mater* 2010; 19: 349–361.
35. Szekrényes A. Interlaminar fracture analysis in the G_{II}-G_{III} plane using prestressed composite beams. *Compos Appl Sci Manuf* 2011; submitted.
36. Reeder JR and Crews Jr JH. Mixed-mode bending method for delamination testing. *AIAA J* 1990; 28: 1270–1276.
37. Szekrényes A. The influence of crack length and delamination width on the mode-III energy release rate of laminated composites. *J Compos Mater* 2011; 59: 279–294.
38. Szekrényes A. Prestressed composite specimen for mixed-mode I/II cracking in laminated materials. *J Reinf Plast Compos* 2010; 29: 3309–3321.
39. Nikbakhta M, Choupani N and Hosseini SR. 2D and 3D interlaminar fracture assessment under mixed-mode loading conditions. *Materials Science and Engineering A* 2009; 516: 162–168.
40. Li X, Carlsson LA and Davies P. Influence of fiber volume fraction on mode III interlaminar fracture toughness of glass/epoxy composites. *Compos Sci Technol* 2004; 64: 1279–1286.
41. Marat-Mendes RM and Freitas MM. Failure criteria for mixed mode delamination in glass fibre epoxy composites. In: *Compos Struct 15th International Conference on Composite Structures*, 2010; Vol. 92, pp.2292–2298.
42. Hashemi S, Kinloch J and Williams JG. Mechanics and mechanisms of delamination in a poly(ether sulphone)-fibre composite. *Compos Sci Technol* 1990; 37: 429–462.
43. Hashemi S, Kinloch J and Williams JG. The effects of geometry, rate and temperature on mode I, mode II and mixed-mode I/II interlaminar fracture toughness of carbon-fibre/poly(ether-ether ketone) composites. *J Compos Mater* 1990; 24: 918–956.